Journal of Hydrology 561 (2018) 223–235

Contents lists available at ScienceDirect

Journal of Hydrology

journal homepage: www.elsevier.com/locate/jhydrol

Research papers

3D mapping, hydrodynamics and modelling of the freshwater-brine mixing zone in salt flats similar to the Salar de Atacama (Chile)

M.A. Marazuela[a,b,c,*], E. Vázquez-Suñé[a], E. Custodio[b,d], T. Palma[a,b,c], A. García-Gil[e], C. Ayora[a]

[a] Institute of Environmental Assessment and Water Research (IDAEA), CSIC, Jordi Girona 18-26, 08034 Barcelona, Spain
[b] Department of Civil and Environmental Engineering, Technical University of Catalonia (UPC), Jordi Girona 1-3, 08034 Barcelona, Spain
[c] Associated Unit: Hydrogeology Group (UPC-CSIC), Spain
[d] Royal Academy of Sciences of Spain, Spain
[e] Geological and Mining Institute of Spain (IGME), Manuel Lasala 44, 9° B, 50006 Zaragoza, Spain

ARTICLE INFO

This manuscript was handled by Corrado Corradini, Editor-in-Chief, with the assistance of Rafael Perez Lopez, Associate Editor

Keywords:
Salt flat
Saltwater intrusion
Saline interface
Brine
Groundwater modelling
Aquifer heterogeneity

ABSTRACT

Salt flat brines are a major source of minerals and especially lithium. Moreover, valuable wetlands with delicate ecologies are also commonly present at the margins of salt flats. Therefore, the efficient and sustainable exploitation of the brines they contain requires detailed knowledge about the hydrogeology of the system. A critical issue is the freshwater-brine mixing zone, which develops as a result of the mass balance between the recharged freshwater and the evaporating brine.

The complex processes occurring in salt flats require a three-dimensional (3D) approach to assess the mixing zone geometry. In this study, a 3D map of the mixing zone in a salt flat is presented, using the Salar de Atacama as an example. This mapping procedure is proposed as the basis of computationally efficient three-dimensional numerical models, provided that the hydraulic heads of freshwater and mixed waters are corrected based on their density variations to convert them into brine heads. After this correction, the locations of lagoons and wetlands that are characteristic of the marginal zones of the salt flats coincide with the regional minimum water (brine) heads.

The different morphologies of the mixing zone resulting from this 3D mapping have been interpreted using a two-dimensional (2D) flow and transport numerical model of an idealized cross-section of the mixing zone. The result of the model shows a slope of the mixing zone that is similar to that obtained by 3D mapping and lower than in previous models. To explain this geometry, the 2D model was used to evaluate the effects of heterogeneity in the mixing zone geometry. The higher the permeability of the upper aquifer is, the lower the slope and the shallower the mixing zone become. This occurs because most of the freshwater lateral recharge flows through the upper aquifer due to its much higher transmissivity, thus reducing the freshwater head. The presence of a few meters of highly permeable materials in the upper part of these hydrogeological systems, such as alluvial fans or karstified evaporites that are frequently associated with the salt flats, is enough to greatly modify the geometry of the saline interface.

1. Introduction

Salt flats (*salares*) are an important source of minerals. They account for half of the world's lithium production and contain the main economic reserves of this element (USGS, 2017). In addition, boron and potash are economically mined from salt flats. Lithium is a strategic commodity; its uses vary from light batteries to cancer treatment. Its demand has notably increased in the last decade, and this trend will probably continue in the future (Vikström et al., 2013), as large quantities may be needed to develop nuclear fusion reactors using tritium generated from lithium. This fact is evidenced by the large number of countries that are just now commissioning studies to determine the mineral potential of their salt flats (e.g., Salar de Uyuni in Bolivia or Salar del Hombre Muerto in Argentina) as well as to increase the amounts of resources that could be exploited during current mining activities (e.g., Salar de Atacama in Chile). This explains the current worldwide interest in salt flat hydrogeology, which is also due to the existence of peripheral brine and saline water lagoons that have high ecological, human and tourist value, in addition to their scientific value.

Salt flats are endorheic lagoon systems associated with arid or hyperarid climates, where the rate of evaporation is very high; in many

* Corresponding author at: Institute of Environmental Assessment and Water Research (IDAEA), CSIC, Jordi Girona 18-26, 08034 Barcelona, Spain.
E-mail address: mamarazuela@outlook.com (M.A. Marazuela).

https://doi.org/10.1016/j.jhydrol.2018.04.010
Received 2 October 2017; Received in revised form 24 March 2018; Accepted 3 April 2018
Available online 04 April 2018

cases, this causes the surface water to disappear and the water table to lie just below the land surface (Yechieli and Wood, 2002). This characteristic is what triggers the important precipitation or accumulation of high-value industrial minerals (Corenthal et al., 2016; Kesler et al., 2012; Munk et al., 2016; Risacher et al., 2003). In these endorheic basins, it is common for evaporation to be higher than local recharge (Hardie, 1991); thus, some other contribution, which is often groundwater, may compensate for this difference. In the simplest case, ignoring hypothetical deep contributions or inflows from other basins, the only water input to the salt flat system is lateral inflow and direct rainfall (which is minor due to the aridity of the climate), and the only output from the system is evaporation. These factors are all strongly related to climate variability and could potentially be affected by global climate change (Rosen, 1994).

The most accepted hydrogeological model assumes that dense brines produced from surface evaporation overturn and sink in the central area of the salt flat, setting up large-scale convection cells in its nucleus (i.e., the core of the salt flat, which is dominated by halite). These cells return to the surface at the margins of the salt flat, where the brines mix with incoming fresh groundwater in a complex process (Fan et al., 1997; Hamann et al., 2015; Nield et al., 2008; Wood and Sanford, 1990; Wooding et al., 1997). For this reason, the discharge of groundwater essentially occurs at the resulting freshwater-brine mixing zone areas, where lagoons may appear (Duffy and Al-Hassan, 1988; Tejeda et al., 2003). As a result, wetlands are commonly present in the margins of salt flats and are the bases for complex and sensitive ecological habitats surrounded by barren lands.

The contact between two miscible fluids of different densities is characterized by a mixing zone, which is also called a saline interface. This interface results from the dynamic equilibrium of moving fresh- and saltwater (Custodio and Bruggeman, 1987; Custodio and Llamas, 1976; Dentz et al., 2006), where the relationship between the concentrations of both fluids is stoichiometric.

In coastal aquifers, the position and characteristics of the mixing zone are well known, and its upper part coincides with the coastline in water table aquifers (Bear, 1972; Glover, 1959; Werner et al., 2013). In salt flats, where the density contrasts are much greater than those in coastal aquifers, the mixing zone develops as a result of point pressure equilibrium between recharge and evaporated water, but its position and geometry are more difficult to predict. This is because the brine in the salt flats is generated *in situ* as a result of evaporation (Acosta and Custodio, 2008), and recharge and evaporation are strongly subject to climatic oscillations (Tyler et al., 2006). Brine mining can affect the dynamics of the mixing zone in a short period of time, similar to freshwater extraction in coastal aquifers (Oude-Essink, 2001). In the natural state, evaporation occurs in both the salt flat nucleus and the marginal zone, regardless of whether it is a sheet of open water (marginal lagoons) or a shallow water table, which commonly have very irregular spatial distributions.

The need to assess the detailed characteristics of the mixing zone occurs immediately when managing both mineral resources and their associated ecosystems. The best management tool are the numerical models in which the effects of variable density are taken into account. These models are expensive to run in two-dimensional (2D) cases and are currently very difficult to run in three-dimensional (3D) cases at the regional scale (Oude-Essink and Boekelman, 1996). Nevertheless, 3D regional scale models are needed for the management of any hydrogeological system. In the case of coastal systems, this problem is solved in two ways: (1) neglecting the effects of variable density by assuming some simplifications or (2) converting the pressures of marine and variable-density waters into equivalent pressures of freshwater (Lu et al., 2015; Maas and Emke, 1989). The last solution, despite providing only an approximation of the actual situation (Post et al., 2007), is the one that has been chosen to model many coastal systems. However, to date, there is no evidence that any similar methodology has been proposed for the study and management of salt flats. Furthermore, the simplifications that are frequently assumed in coastal aquifers, such as neglecting density variations when advection is dominant over convection (Iribar et al., 1997; Vázquez-Suñé et al., 2006), are not acceptable in salt flats.

To obtain solutions for the above problem, the Salar de Atacama (NE Chile) was chosen as a case study. The choice was based on three characteristics: (1) it is the third largest salt lake on Earth, with a surface area of 3000 km^2; (2) it contains exceptional water ecosystems and bird nesting areas in the surficial mixing zone area, which require scientific solutions for their preservation and sustainability; and (3) there is a unique monitoring network that is regularly operated and well instrumented (Tyler et al., 2006) thanks to the exploitation of brine resources carried out in the southwestern area of the salt flat nucleus.

The main objective of this work is to obtain the first 3D map of the salt flat mixing zone, using the Salar de Atacama as a case study. This 3D map, together with an idealized 2D numerical model, allows us to understand the dynamics of the mixing zone and the effects of heterogeneity on its large-scale geometry. We also propose the use of the 3D map to apply simplified rules for constant-density 3D models that include mixing zones.

The structure of the manuscript follows the order described below. First, the 3D mapping of the mixing zone is addressed. Second, the usefulness of 3D mapping in the salt flats to correct the hydraulic heads by density differences and to facilitate their modelling at a constant density is shown. Third, the idealized 2D numerical model of the regional mixing zone is performed. Fourth, the sensitivity analysis of the hydraulic conductivity of the upper aquifer is carried out to determine its influence on the geometry of the mixing zone on a regional scale.

2. Materials and methods

2.1. Geographic setting

The Salar de Atacama (hereinafter SdA) is located in northern Chile between 23° and 24° South latitudes and 68° and 69° West longitudes; it is located in Region II (Antofagasta) and within the limits of the community (municipality) of San Pedro de Atacama (Fig. 1). The basin where the salt flat is located has an oval shape, with the long axis in the N-S direction and an extent of approximately 20,000 km^2. It is bordered to the west by the Cordillera de la Sal (Salt Range), which stretches from NNE to SSW at the slopes of the Domeyko Range, and to the East by the western Cordillera de los Andes (Andean Range), whose high peaks are crowned by the current volcanic arc (> 5500 m a.s.l., metres above sea level). The northern part of the basin is bounded by the merging of the Domeyko Range and the Andean Range, while the southern part is bounded by the Lila Mountains.

Because the Andean Range acts as a geographic barrier to atmospheric movement, the SdA is characterized by a hyperarid climate, resulting in a very low rainfall rate (Bookhagen and Strecker, 2008; Garreaud et al., 2010; Hartley and Chong, 2002). On average, the salt flat receives less than 20 mm/yr of precipitation. The major water source is groundwater coming from the Andean Range. In the mountains, the average precipitation reaches 160 mm/yr (IDAEA-CSIC, 2017). The output is water table evaporation produced in the nucleus and marginal zone, where the mean surficial water evaporation rate is 4.3 mm/d. Evaporation decreases as the depth of the water table increases, and it depends on the soil composition (Kampf et al., 2005; Kampf and Tyler, 2006; Muñoz-Pardo and Ortiz-Astete, 2004).

The two main river courses contributing to the salt flat, as shown in Fig. 1, are the San Pedro River, which has an average flow of 1 m^3/s and torrential events of up to 25 m^3/s, and the Vilama River, which has an average flow of 0.2 m^3/s. These rivers flow from North to South (Salas et al., 2010). The San Pedro River ends in a delta with the same name, while the Vilama River disappears in the upper half of its basin. There are also some intermittent streams that descend from the mountains and infiltrate into the extensive alluvial fans on the eastern side of the

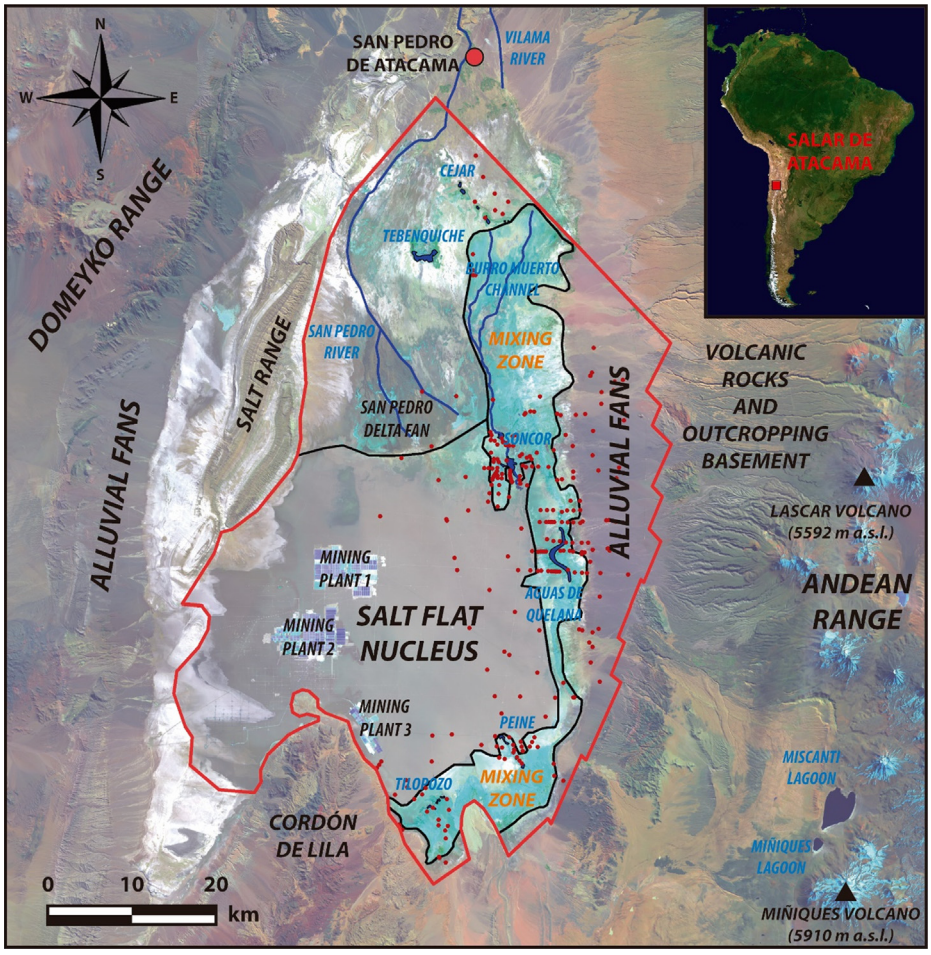

Fig. 1. Location of the SdA (LANDSAT 8, 27 September 2016). The main geological and geographical domains are shown in black lettering; rivers, channels and water systems are shown in blue lettering. The saline interface or mixing zone are shown as black lines and orange lettering. Red points are the observation points used for the 3D mapping of the mixing zone.

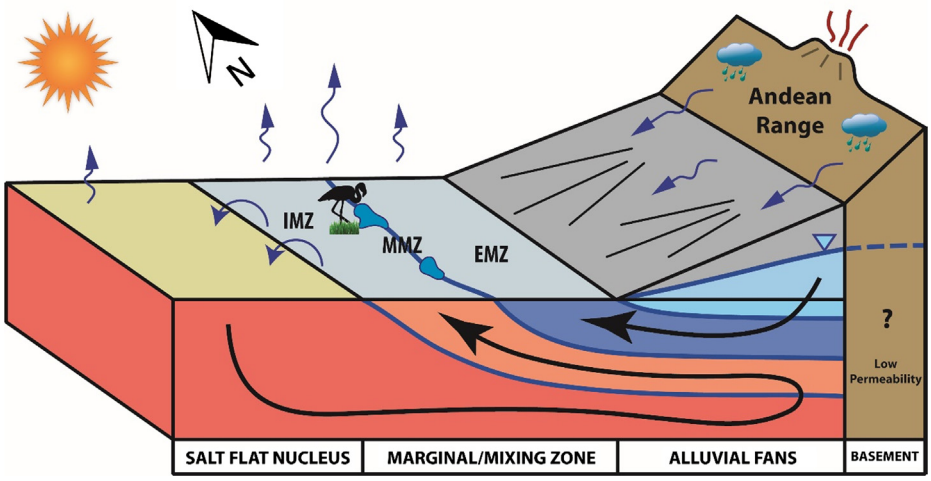

Fig. 2. Conceptual model of the mixing zone in the Salar de Atacama. Black lines represent the flow paths. IMZ - Internal mixing zone; MMZ - Middle mixing zone; EMZ - External mixing zone.

salt flat. In many cases, these streams are controlled by structural features.

In addition, in the eastern margin (surficial mixing zone) of the SdA, there are many lagoons and wetlands; in some cases, these have been defined as Ramsar sites. This area has been recognized by the international community as an environment with significant value for humanity. Some lagoons reach surface areas of several hectares, although most are smaller. The lagoons are grouped into four systems (Fig. 1): Soncor (Chaxa, Barros Negros and Puilar lagoons), which is connected by the Burro Muerto channel; Aguas de Quelana; Peine (Salada, Saladita and Interna lagoons); and Tilopozo (La Punta and La Brava lagoons). These lagoons are the habitats for several migratory or

endemic species, mainly birds, among which there are three species of high Andean flamingos, xerophytic and halophytic shrubs or grass, and some mammals, microcrustaceans, microalgae and bacteria.

Flamingos mainly feed on microcrustaceans (e.g., *Artemia*), whose range of vital salinity has more or less defined thresholds. Outside these limits, the population of this biota is reduced due to its inability to reproduce and survive if the salt concentration increases or to compete with new predators if the concentration of dissolved salts decreases (Gajardo and Beardmore, 2012).

2.2. Hydrogeological framework

The SdA is currently located in a compressive tectonic basin, which is framed by inverse faults which affect from the Palaeozoic basement to present deposits (Arriagada et al., 2006; Jordan et al., 2007; Mpodozis et al., 2005). Based on its geomorphological, geological and hydrogeological characteristics, four large domains can be distinguished from the watershed line to the basin depocenter (Figs. 1 and 2): 1) the basement and the volcanic deposits of the mountain range, 2) the alluvial fans descending therefrom, 3) the marginal zone (2300 to 2320 m a.s.l.) and 4) the SdA nucleus (2300 m a.s.l.).

In the actual basin depocenter (i.e. the halite nucleus), a series of clastic and evaporitic sediments are known to have been deposited from the Upper Miocene to the present, with a thickness that exceeds 1400 m in some areas (Jordan et al., 2007; Mpodozis et al., 2005; Pananont et al., 2004). The evaporite deposits in the nucleus and marginal zone show a well-defined asymmetric zonation that follows a sequence of classic evaporite precipitation, with a gradual evolution from carbonates and sulphates in the marginal zone to halite in the salt flat nucleus (Vásquez et al., 2013), where solutes of mining interest are concentrated in the remnant final brines.

Alluvial deposits and some layers of the salt flat nucleus have medium to high hydraulic conductivities (IDAEA-CSIC, 2017; Muñoz-Pardo and Ortiz-Astete, 2004; Rockwood Lithium, 2015). In the alluvial deposits, this is due to their primary lithological properties; in the salt flat nucleus, this is the result of intense karstification processes. In the salt flat, the main aquifer is the upper layer of halite (60–300 m/d). There is also a deeper second halite aquifer (0.1–20 m/d), which is confined by a layer of low-permeability gypsum acting as an intermediate aquitard (0.01–5 m/d). This same aquifer-aquitard-aquifer sequence applies to the alluvial fans as a regional simplification, where the upper (80–300 m/d) and lower (20 m/d) high-permeability detrital deposits are separated from the lower ones by some relatively poorly permeable layers (0.01–5 m/d).

The regional potentiometric surface shows a concentric flow that extends from the highest areas to the depocenter of the basin. Due to the low recharge and topography, the water head gradients are very small (less than0.001 m/m), especially in the nucleus and marginal zones, where these gradients are almost zero. In the marginal zone (mixing zone), groundwater crops out, thus indicating the freshwater-brine interface zone (Fig. 2).

2.3. Hydraulic role of the mixing zone in the lagoons and wetlands of the Salar de Atacama

Three hydraulic domains have been distinguished in the mixing zone, from the eastern boundary of the salt flat nucleus to the lateral alluvial fans. These are the internal (IMZ), middle (MMZ) and external (EMZ) mixing zones (Fig. 2).

Freshwater recharge is mainly produced on the eastern mountain side. The marginal lagoons, wetlands and springs are located in the MMZ (Fig. 2). The resulting flow discharges into this zone and ascends to the surface, resulting in the Quelana, Peine and Tilopozo lagoons. The Soncor lagoon system is a special case, as it is located in the IMZ and not in the MMZ; its origin is not the direct groundwater overflow of the MMZ (Ortiz et al., 2014). Along the final flow path, the total dissolved solids (TDS) of the groundwater gradually increase as a consequence of mixing and evaporation, as it is very shallow. Some of the water returns to the IMZ and the salt flat nucleus as concentrated brine (Fig. 2). This dynamic behaviour is strongly variable due to the seasonality of recharge and evaporation (Salas et al., 2010).

2.4. Hydrogeological data

The analysis of satellite images (LANDSAT 8) allows us to map the surface hydrological features and the mixing-zone geometry near the land surface.

Water heads and physico-chemical parameters (e.g., electrical conductivity) were measured in the field. The same physico-chemical parameters and solute concentrations were measured in the laboratory following standard procedures. Some vertical electrical conductivity (EC) profiles were obtained in boreholes. Data are available from a total of 310 observation points (wells, piezometers, trenches and surface water courses) distributed throughout the area (Fig. 1), with records dating back to 1984. Most of the data used for this research project were provided by the SQM Company. These data have been complemented with other difficult-to-access sources of information (Rio Chilex S.A, 1997; Rockwood Lithium, 2015). The main information of the wells with physico-chemical data (coordinates and average values of EC, density and salinity) is compiled in Table S1 Of The Supporting Information.

The monitoring network consists of well-levelled points with which to measure the water head and collect water samples. These monitoring points are most often boreholes, but they often designed as wells and piezometers. Some boreholes are point wells, which are open or screened in a short interval at a given depth, but they often have long open and screened sections. The cased section of the piezometer may contain water of a different density and salinity than that in the open part (Rushton, 1980). This affects the measured water head. This effect can be corrected by obtaining an electrical conductivity (EC) log to calculate vertical density changes and introduce the needed corrections; it can also be corrected by substituting the water inside the borehole before measuring the level for water in the open section by repeated bailing or low-flow pumping from near the water surface. Nevertheless, in low-permeability layers, this measurement may be distorted by residual water level drawdown. In most cases, the depth to the water level is measured without considering the salinity in the uncased section. This may introduce some errors in marginal areas with great vertical salinity gradients and where shallow water may enter the borehole. Water samples are often collected using a bailer or a thief sampler that opens at the desired depth. Some mixing may thus occur with other water in the borehole or pit. The best water samples are obtained with a low-flow pump with the inflow inside the section to be sampled. Measuring and sampling protocols are applied.

To increase the number of available data points, correlations between density, EC and TDS were obtained (Fig. 3). Their magnitudes show a clear mutual correlation (Kohfahl et al., 2015) and provide a practical technique with which to map the interface. For EC measurements, it is necessary to apply a correction for temperature (T) (Hayashi, 2004) of approximately 2%/°C, if it is not automatically done when EC and T are measured. The EC correction and probe calibration errors may also explain part of the dispersion. The correlation between density and EC is not linear and follows a more complex polynomial line. The correlation between TDS and EC shows linear behaviour up to 100 $mS \cdot cm^{-1}$, similar to other brines (Jellison et al., 1999); however, for higher EC values, the correlation is nonlinear, which will increase dispersion if a polynomial relationship is not applied.

2.5. Darcy's law, head and pressure formulation in variable-density flow

Calculating flow directions and flow rates is the basic goal of almost all hydrogeological studies. These values can be obtained using Darcy's

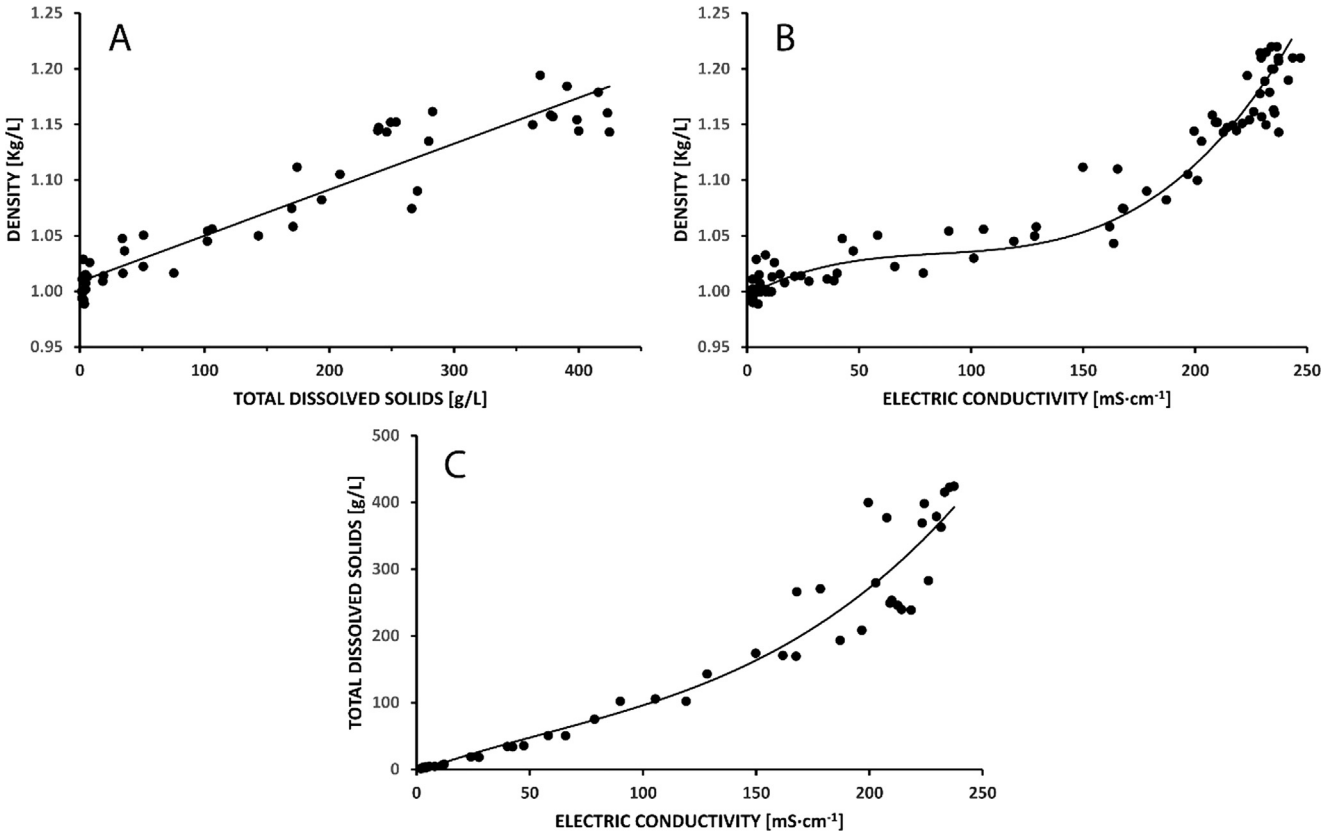

Fig. 3. (A) Correlation between total dissolved solids (TDS) and density; (B) correlation between electrical conductivity (EC) and density; and (C) correlation between electrical conductivity and TDS. The black line shows the best-fit curve for both correlations.

law. In the case of variable density, the Darcy's law in terms of water pressure is (Bear, 1972):

$$\mathbf{q} = -\frac{\mathbf{k}}{\mu}(\nabla\ \mathrm{P} + \rho g \nabla z) \tag{4}$$

where $\mathbf{k}$ is the intrinsic permeability tensor, μ is the fluid viscosity, P is the pressure, ρ is the fluid density and g is the gravitational acceleration and ∇z denotes the vertical upward direction. The spatial components of $\mathbf{q}$ are:

$$\mathbf{q_x} = -\frac{k}{\mu}\frac{\partial P}{\partial x} \tag{5}$$

$$\mathbf{q_y} = -\frac{k}{\mu}\frac{\partial P}{\partial y} \tag{6}$$

$$\mathbf{q_z} = -\frac{k}{\mu}\left(\frac{\partial P}{\partial z} + \rho g\right) \tag{7}$$

The horizontal flow components, $\mathbf{q}_x$ and $\mathbf{q}_y$, can be calculated based on the corresponding horizontal components of the pressure gradients or from the head gradients referring to the same water density.

For vertical flow, $\mathbf{q}_z$, there is a buoyant term associated with the gravity vector, which does not appear in the horizontal directions.

2.6. Numerical approach

A variable-density flow pattern is the result of strongly coupled flow and mass transport differential equations. Flow in porous media can be described using the following water mass conservation differential equation:

$$S_s\frac{\partial h}{\partial t} + \nabla\cdot\mathbf{q} = 0 \tag{8}$$

where S_s is the specific storage, and t is the time.

Neglecting all density dependencies in the balance terms except for the buoyancy term (the Oberbeck-Boussinesq approximation), $\mathbf{q}$ is given by the following expression in terms of water heads:

$$\mathbf{q} = -\frac{\mathbf{k}\rho_0 g}{\mu}\frac{\mu_0}{\mu}(\nabla\ \mathrm{h} + \frac{\rho-\rho_0}{\rho_0}\nabla z) \tag{9}$$

Note that ∇z is multiplied by the density ratio in which ρ_0 is the reference water density. The viscosity relation function, where μ_0 is the reference fluid viscosity, may be neglected in viscosity constant models.

Salt transport can be described using the differential equation:

$$\phi\frac{\partial C}{\partial t} + \mathbf{q}\cdot\nabla\ \mathrm{C} + \nabla\cdot(-\mathbf{D}\nabla \mathrm{C}) = 0 \tag{10}$$

where porosity is ϕ, solute concentration is C, and the hydrodynamic dispersion tensor is $\mathbf{D}$.

The code FEFLOW was used to solve this set of coupled governing equations. More information about the formulation and performance of this code can be found in Diersch (2014).

3. Results

3.1. 3D mapping of the freshwater-brine mixing zone

The central axis of the mixing zone at the surface was identified through the use of satellite images (Fig. 4). This axis coincides with wetlands and small, easily recognizable seasonal lagoons (Tejeda et al., 2003).

The three-dimensional mapping of the main mixing zone was performed by identifying the position of its central surface (EC = 150 mS·cm^{-1}), upper surface (EC = 100 mS·cm^{-1}) and lower surface (EC = 200 mS·cm^{-1}). These surfaces are used to delineate the

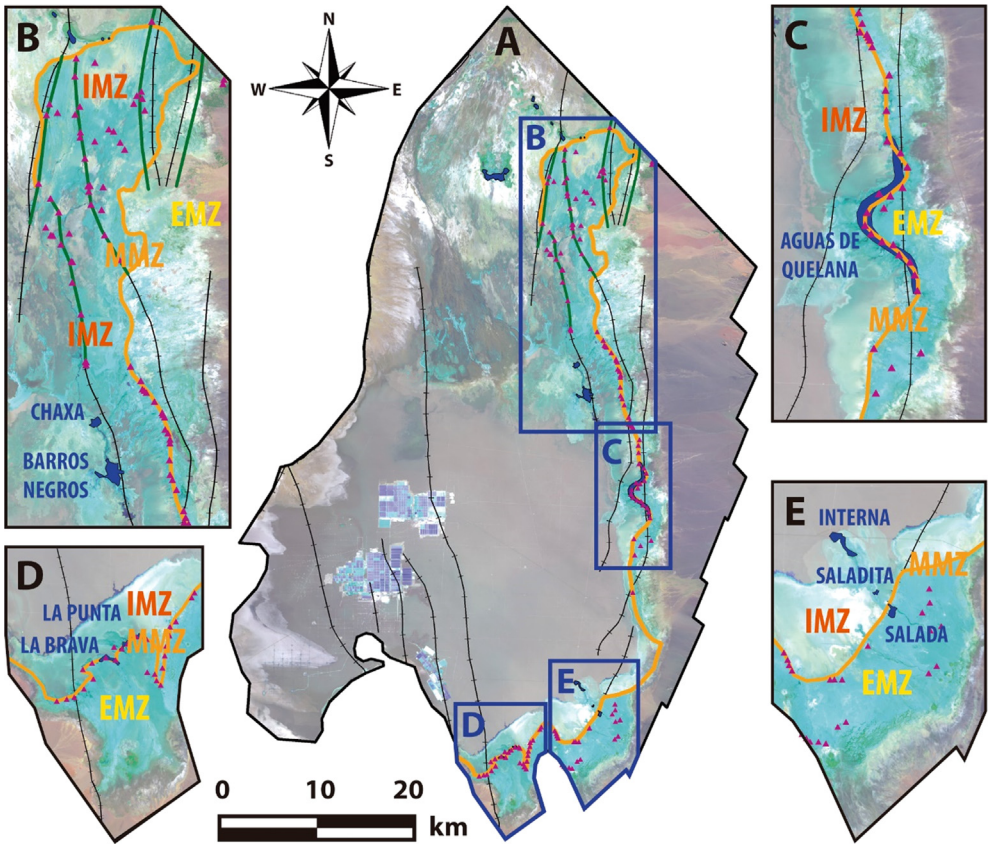

Fig. 4. Surficial mixing zone mapping of the SdA. (A) General mixing zone framework. The orange line is the middle mixing zone (MMZ); the purple triangles are springs; the black lines with small cross lines are the faults described by Universidad de Chile (2016), and the green lines are the proposed extensions of these faults, which coincide with numerous springs in the IMZ. The dark blue rectangles show the positions of figures B, C, D and E. (B) Mixing zone of the north and Soncor lagoon systems; it highlights the structural controls (faults and fractures) on the springs; words in red, orange and yellow indicate the internal (IMZ), middle (MMZ) and external (EMZ) mixing zones, respectively. (C) Eastern area of the surficial mixing zone, with the Aguas de Quelana lagoon system. (D) Mixing zone of the southeast area of Peine (Salada, Saladita and Interna lagoons). (E) Mixing zone of the southwestern area of Tilopozo (La Brava and La Punta lagoons).

main mixing zone, which is the region in which the salinity gradient changes most rapidly. The given limits do not represent the extreme EC values corresponding to brine and freshwater. Values between 200 and 240 mS·cm^{-1} are only reached in the central area of the nucleus, and values of less than a few mS·cm^{-1} are reached in the recharge areas.

The position of the mixing zone was deduced based on the density data measured or calculated in each piezometer. Using nests of wells, where each one is open at a different depth, allows the more faithful characterization of the geometry of the mixing zone. Nevertheless, considering the particular characteristics of each monitoring point, the majority of these sites could be used to produce valuable information.

The SdA mixing zone mainly extends throughout the Northeast, East and Southeast salt flat margins (Figs. 5 and 6). The full range of densities present in the mixing zone can be observed on the land surface. The surficial densities closest to 1.23 kg/L were measured in the salt flat nucleus, while the densities closest to 1 kg/L were measured in the external mixing zone and the recharge zone. The mixing zone shows a moderate slope in the IMZ (internal mixing zone), strong deepening in the MMZ (middle mixing zone) and a gradual slope reduction in the EMZ (external mixing zone) and recharge areas. The external limits have been defined as far away as possible, as monitoring wells are very scarce. It is expected that the interface will extend beyond these limits but that it will have a low slope.

3.2. 2D numerical model of the Salar de Atacama mixing zone

An idealized vertical profile 2D numerical model was carried out to use it as a tool to understand the geometry of the mixing zone. Although great local heterogeneity has been described in the Salar de Atacama (Muñoz-Pardo and Ortiz-Astete, 2004; Ortiz et al., 2014; Salas et al., 2010), only three simplified layers have been considered for the idealized regional model (Fig. 7). These layers attempt to represent the regional aquifer-aquitard-aquifer sequence that has often been identified in both the salt flat nucleus and the alluvial fans. As shown in the pumping tests done in the region, the hydraulic contrast between these three units (aquifer A, aquitard AB and aquifer B) is conspicuous and spatially continuous, but the hydraulic conductivity values may vary due to heterogeneities and karstification (IDAEA-CSIC, 2017).

The model domain represents an idealized vertical cross-section that is 25,000 m long and 1200 m high (Fig. 7). The length is the characteristic of any section of the eastern mixing zone, including 10,000 m of nucleus, 5000 m of mixing zone and 10,000 m of alluvial fans. The thickness chosen corresponds to the thickness of the nucleus (Vilama Formation) in the eastern area (Jordan et al., 2007). The right boundary is the contact between the basement rocks and alluvial fans that may be considered impermeable in a simplification because the water that falls in the mountains (volcanic rocks and basement of low permeability) reaches the alluvial fans largely superficially, where it infiltrates due to their greater permeability; the left boundary is located inside the salt flat, similar to other models (Duffy and Al-Hassan, 1988; Fan et al., 1997; Hamann et al., 2015); the lower boundary is located at the bottom of the geological unit B; and the upper boundary is the water table. Aquifers are modelled as confined aquifers (with constant transmissivity) because the water table variations are very small compared to the aquifer thickness due to the very low hydraulic gradients. The model mesh has approximately 153,000 triangular elements.

To model the salt flats, two main methodologies are used, depending on the objective for which the model is constructed. To study the geochemistry or detailed evaporation processes of the salt flat, reactive transport models can be carried out that include evaporation and dissolution using well-established saturation indices (Hamann et al., 2015; Vásquez et al., 2013). However, this coupling requires extremely high calculation times even for idealized problems (Hamann et al., 2015); thus, techniques are often used that simplify the problem numerically without altering the geometry of the resulting mixing zone (Duffy and Al-Hassan, 1988; Fan et al., 1997). In this way, it is possible to limit the maximum density without needing to precipitate salts based on saturation indices.

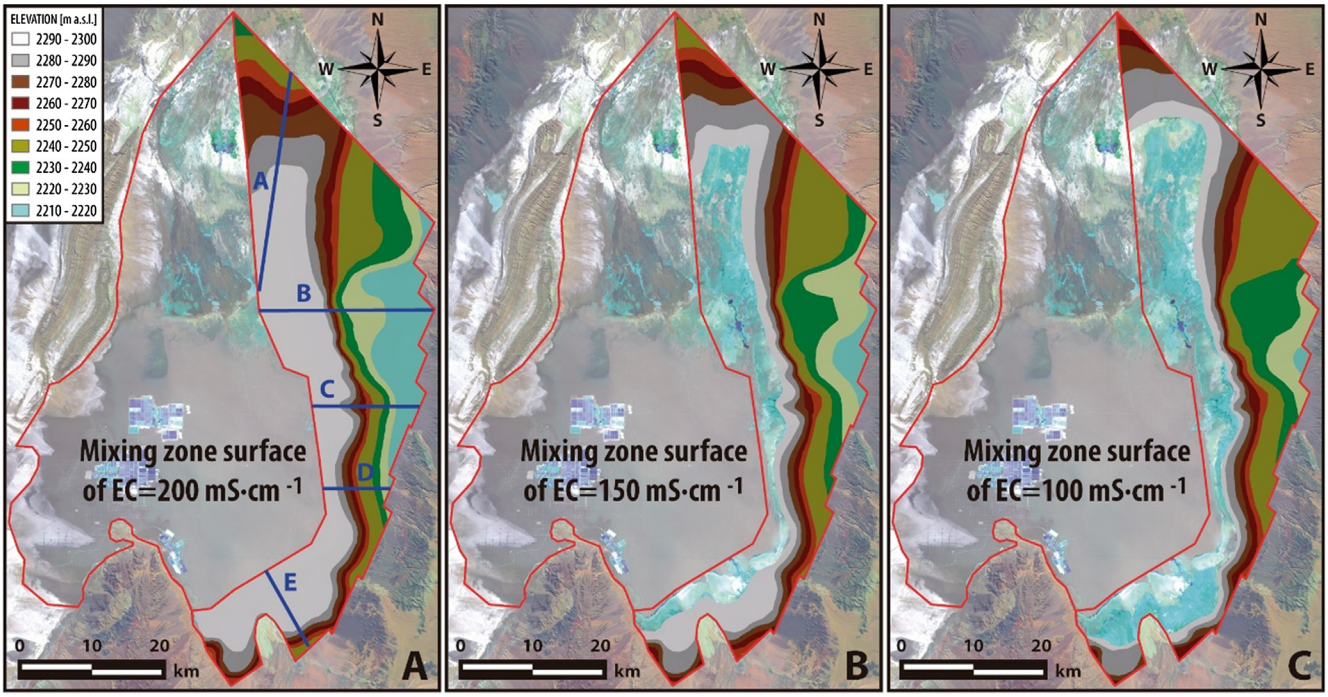

Fig. 5. Three-dimensional mapping of the mixing-zone control surfaces. (A) Surface of 200 mS·cm^{-1}. (B) Surface of 150 mS·cm^{-1}. (C) Surface of 100 mS·cm^{-1}. The blue lines show the locations of the cross-sections in Fig. 6.

Following these guidelines, the left, lower and right boundaries are treated as no-flow zones for water and mass (i.e., Neumann-type boundary conditions).

At the top, different boundary conditions are selected for each spatial stretch with the purpose of representing the evaporation and recharge processes. The reference values of recharge were taken from IDAEA-CSIC (2017). The recharge, considering the total length (36.25 km) from the distal alluvial fans to the watershed line, ranges from 20 to 140 mm/yr, respectively. If a detention of 25% is considered, then the net recharge rate ranges from 15 to 105 mm/yr. But in our simplified model we only considered 10 km of the total recharge length. By this motive, a fluid inflow (Neumann-type boundary condition) was fixed on the recharge surface, with a minimum value of 15 mm/yr in the contact between the mixing zone and the alluvial fans and a maximum value of 420 mm/yr (an unrealistic recharge rate that allows the model to enter the total recharge volume) in the contact between the alluvial fans and the basement. As in previous models (Duffy and Al-Hassan, 1988; Fan et al., 1997) the recharge was applied on the top to not condition the mixing zone in the right boundary. This takes advantage of a large part of the water recharged in the mountains infiltrates the alluvial fans. A water head (Dirichlet) was fixed in the halite nucleus and the internal mixing zone.

For mass transport, fixed solute concentration of 1.23 kg/L for the salt flat nucleus and 1.00 kg/L for the freshwater recharge area were implemented. Concentrations were normalized to the densities of freshwater and brine as end members.

The upwinding option for the numerical treatment has been used to smoothen out steep concentration changes, although this causes some additional numerical dispersivity.

A stationary simulation was carried out to obtain the initial water heads. For the initial mass condition, a concentration of 1.00 kg/L was assigned, corresponding to a hypothetical initial scenario where all groundwater is fresh. The model was run for several thousands of years, with a semiautomatic time-step control, to reach a quasi-stationary state. The hydraulic parameters deduced from pumping tests, or in some cases from the literature (IDAEA-CSIC, 2017), are given in Fig. 7.

The results are shown in Fig. 8. The geometry of the mixing zone in accordance with the 2D numerical model and the 3D mapping presents a very small slope which allows it to penetrate through all of the alluvial fans. Only in the first section (between the nucleus and the alluvial fans) is the interface slope greater. This type of mixing zone corresponds to arid and high-permeability salt flats, in accordance with the case 4 described by Duffy and Al-Hassan (1988).

3.3. Comparison with analytic solutions for the sharp interface in coastal aquifers

A comparison of the results of the model with the most commonly used analytical solutions in coastal aquifers is made below.

In the case of a sharp interface, the freshwater and saltwater pressures must be equal at the interface. The Badon-Ghyben-Herzberg (BGH) principle (Custodio and Bruggeman, 1987; Custodio and Llamas, 1976) establishes that in a homogeneous coastal aquifer, the depth of the interface below sea level ξ is given as $\xi = \alpha h_f$, in which h_f is the freshwater head and α is the inverse of the relative density difference: $\alpha = \rho_f/(\rho_s - \rho_f)$ where ρ_s and ρ_f are the densities of saline water and freshwater, respectively. It is assumed that the freshwater flow is horizontal and that the saline water flow is steady and equal to that of the saline water body. For coastal aquifers, the most frequent value of α is 40. For the Salar de Atacama brine, the value of α is 4.35. As vertical flows and the true brine head are not taken into account in the BGH principle, the predicted depth is generally too shallow, and it does not occur inside the actual mixing zone. Therefore, in most cases, the BGH formula is not a good predictor of the mixing zone depth.

If the actual head of salt water is considered, the Hubbert (1940) formula is used:

$$\xi = \alpha h_f - (1 + \alpha) h_s \quad (1)$$

where h_f and h_s are theoretically measured on the interface. In practice, they are assumed to be equal to the freshwater and saline water heads measured in the point monitoring wells on the vertical axis of the site considered or near it. Thus, vertical components are ignored, which introduces an error. The closer the well screens are to the mixing zone, the more the predicted position generally falls inside or closer to the

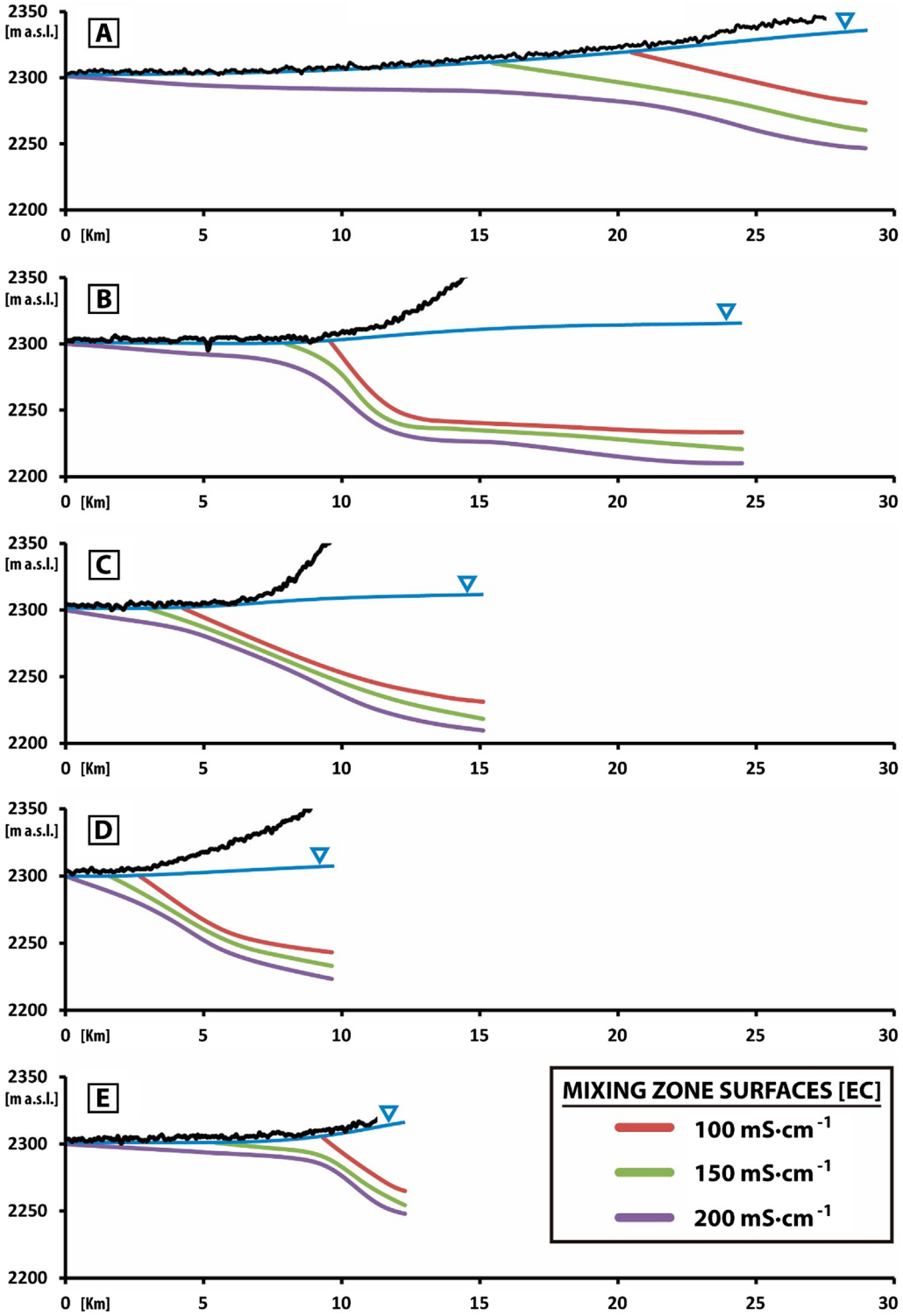

Fig. 6. Cross-sections of the mixing zone. In figures B, C and D the upper vertical scale has been limited to 2350 m a.s.l. for enhanced clarity. The locations of the profiles are shown in Fig. 5. The black line corresponds to the topography, and the blue line corresponds to the water table.

position of the mixing zone.

Pool and Carrera (2011) proposed an empirical improvement of the BGH principle for coastal aquifers in which $\varepsilon = 1/\alpha = (\rho_s - \rho_f)/\rho_f$ is changed to $\varepsilon^* = [1-(\alpha_T/b')^{1/6}]$, in which α_T = transversal dispersivity and, b' = depth below sea level of the aquifer bottom, which is assumed to be horizontal. They rewrote the BGH approximation to the interface depth as $\xi = h_f/\varepsilon^*$.

None of these predictions take into account the effect of layering, which is very important in the case described here.

In the case study, the sharp BGH interface is always situated well above the mean mixing zone surface (1.115 kg/L) (Fig. 8). The sharp interface resulting from the Pool and Carrera (2011) approximation shows a better fit of the mixing zone. The Hubert interface best fits the results of the numerical model, although it requires a greater number of hydraulic head data for its calculation, which hinders its practical applicability.

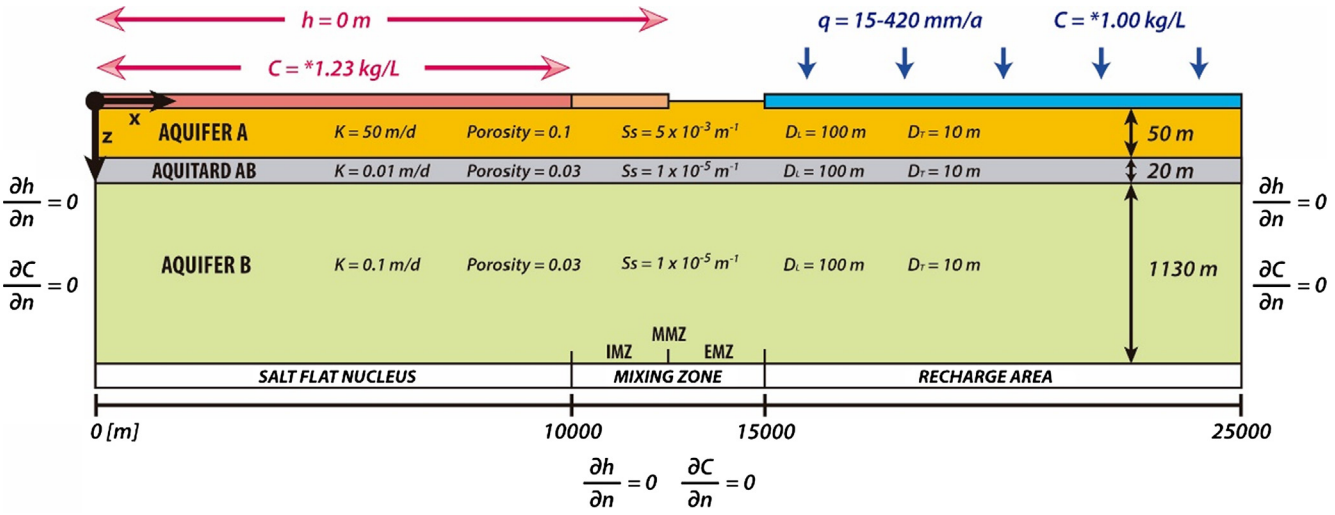

Fig. 7. Geometry, boundary conditions and hydraulic properties used in the two-dimensional numerical model. The boundary conditions are shown in blue for the recharge area and in red and orange for the evaporation area. D_L and D_T are the longitudinal and transversal dispersivities, respectively. The hydraulic conductivity (K) of the aquifer A was modified during the sensitivity analysis described in the text. The concentration values (*) were normalized to the density value.

4. Discussion

4.1. Water head corrections by contrast densities in salt flats

In the case of SdA, only a few potentiometric surface mappings were completed in previous studies. Moreover, only some simplified three-dimensional numerical modelling has been performed, none of which was at the regional scale and they often neglected the effects of density. Muñoz-Pardo and Ortiz-Astete (2004) performed a 3D numerical model of the nucleus and marginal zone of the SdA by neglecting density effects, although they recognized a range of densities between 0.99 and 1.22 kg/L. Ortiz et al. (2014) also showed a potentiometric surface mapping of the Soncor lagoons system without taking density effects into account. Salas et al. (2010) were the only authors to consider the effects of density although they did not explain the followed methodology. In that study, the flow path lines did not describe the expected behaviour of a natural freshwater-brine mixing zone because at the time of that study the brine pumps had already depressed the water table in the nucleus.

Establishing the direction and sense of the water flow directly from the water head data measured in piezometers and wells with waters of different salinities is often erroneous. This error may be very important if the contrast in densities is as important as it is in the SdA. Thus, all water head measurements have been transformed to the same reference density, and these were subsequently used following the rules of considering consider buoyancy effects.

In the case of salt flats, especially in the nucleus, marginal zone and its surroundings areas, the dominant flow component is vertical, unlike that in coastal aquifers. Therefore, it is essential to apply a correction allowing for the most faithful reproduction possible of the vertical flow near the mixing zone. If the density dependence of the flow is neglected, the predicted flow path lines have their origin in the mountains and end

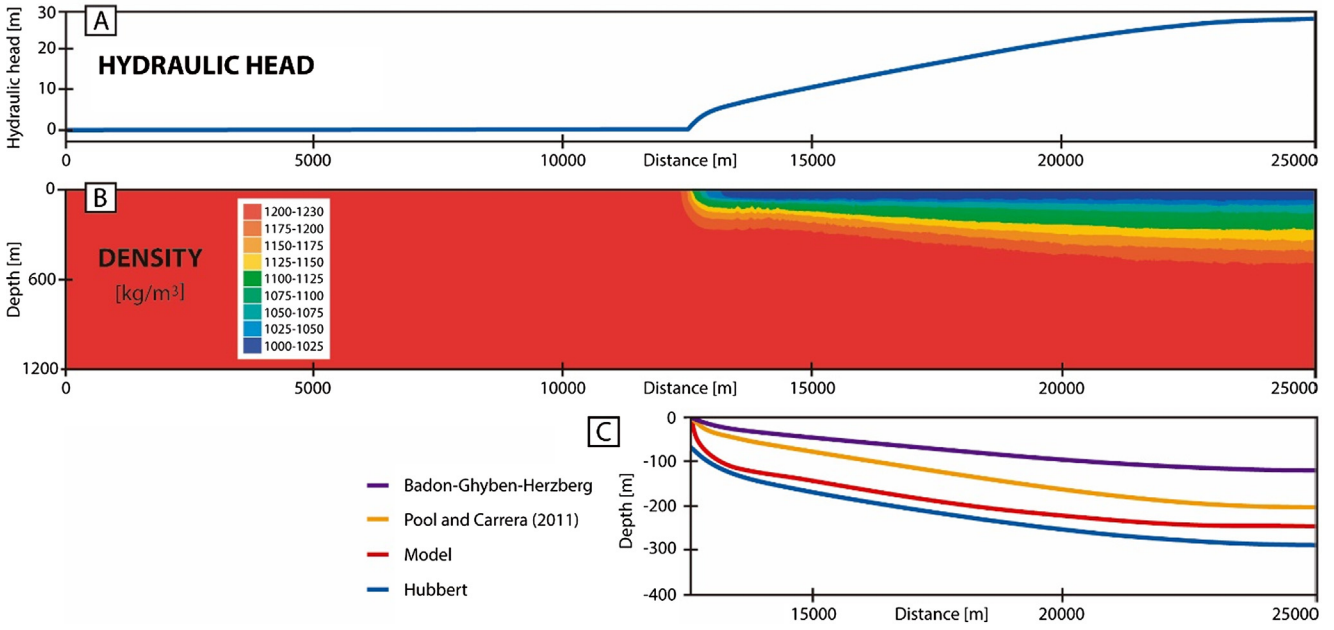

Fig. 8. Results of the idealized 2D numerical model. (A) Computed hydraulic heads of the top boundary, relative to the mean altitude of the nucleus. (B) Resulting densities. (C) Comparison between the modelled mixing zone and the three main analytical solutions for the mixing zone in homogeneous coastal aquifers. Badon-Ghyben-Herzberg (BGH), Hubbert, and Pool and Carrera (2011). The vertical scale was exaggerated by a factor of three.

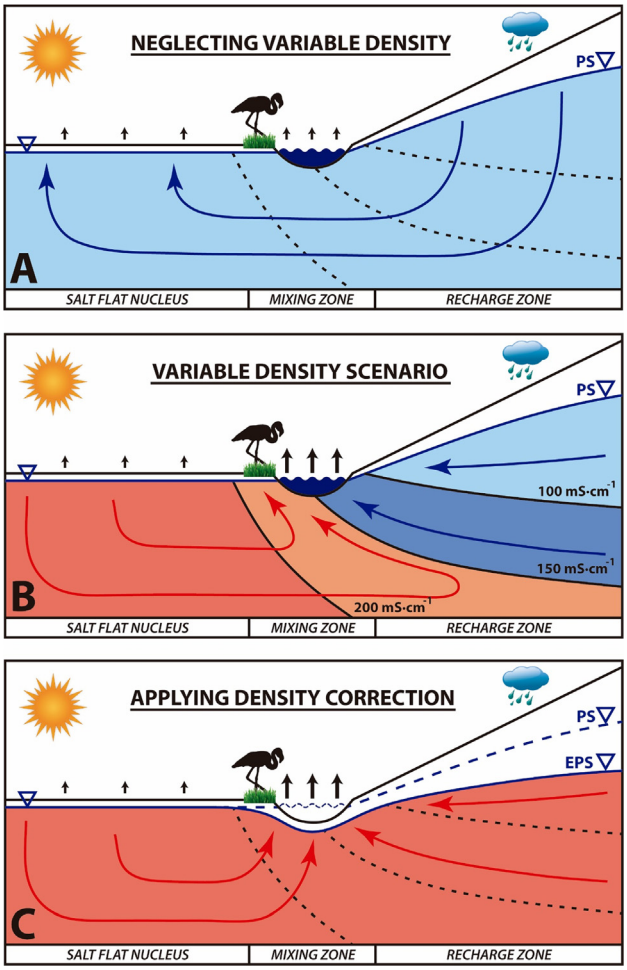

Fig. 9. (A) Flow dynamics if density variations in groundwater are totally neglected. (B) Actual situation of the surficial mixing zone, with freshwater (light blue), brine (dark orange) and intermediate water (dark blue and light orange colours). (C) Flow dynamics if density corrections to the potentiometric surface are applied. The mixing zone lagoons at the minimum regional water head clearly stand out. PS is the potentiometric surface and EPS is the corrected potentiometric surface.

in the salt flat nucleus (Fig. 9A). This contrasts with a general observation in which groundwater discharge and wetlands occur at the margins of the salt flats (Fig. 9B). However, taking into account the effects of density on flow in three-dimensional complex numerical modelling is almost impossible because of the high degree of computational power that is required.

An interesting solution would be to apply a density-correction methodology similar to that applied to coastal aquifers (Lusczynski, 1961) to transform saltwater heads into freshwater heads. The results obtained using this methodology indicate that the lagoons are in the regional minimum water head and that they represent the main discharge area, similar to the actual case (Fig. 9C). Nevertheless, in contrast to coastal aquifers, the focus of interest and the highest numbers of observation points in salt flats are in the nucleus and the mixing zone but not in the freshwater zone (recharge area). For this reason, it is much more useful to develop a solution that allows for the correction of the water heads by transforming freshwater heads into brine heads.

The following procedure is adopted for the water head correction depending on the characteristics and available information obtained from piezometers or wells. Four study cases have been established: point wells with an EC profile, long-screened wells with an EC profile, point wells without an EC profile, and long-screened wells without an EC profile.

The point wells, slotted only in a very short stretch, in which an EC profile was available have been corrected by taking the vertical density distribution into account using the equation:

$$h_c = h_i + \int_{z_0}^{z_2} z\frac{\rho-\rho_0}{\rho_0}dz \quad (2)$$

where h_c is the corrected water head, h_i is the measured water head, z is the saturated well thickness, z_0 is the origin of the water depths of the well, z_2 is the depth corresponding to an EC of 200 mS·cm^{-1}, ρ is the density measured at each point and ρ_0 is the reference density. In the case of SdA, the reference density is 1.23 kg/L.

The long-screened wells with an EC profile were corrected using the same criteria. A unitary correction for each stretch of the vertical profile may be performed by obtaining the vertical distribution of the water heads.

The point wells in which an EC profile was not available were corrected assuming that the slotted density was homogeneous throughout the entire well. In this case, the previous equation is simplified to:

$$h_c = h_i + z\frac{\rho-\rho_0}{\rho_0} \quad (2)$$

The long-screened wells without an EC profile were corrected by assuming the density distribution of the reference EC/density surfaces obtained in the regional mixing zone mapping (Fig. 10). To apply the correction in each piezometer, three stretches are considered inside these monitoring wells: 1) the thickness of the water layer below the surface of 200 mS·cm^{-1}; 2) the thickness between the surfaces of 200 mS·cm^{-1} and 100 mS·cm^{-1}, with a reference surface of 150 mS·cm^{-1}; and 3) the thickness between the surface of 100 mS·cm^{-1}; and the water table. The first stretch is not corrected

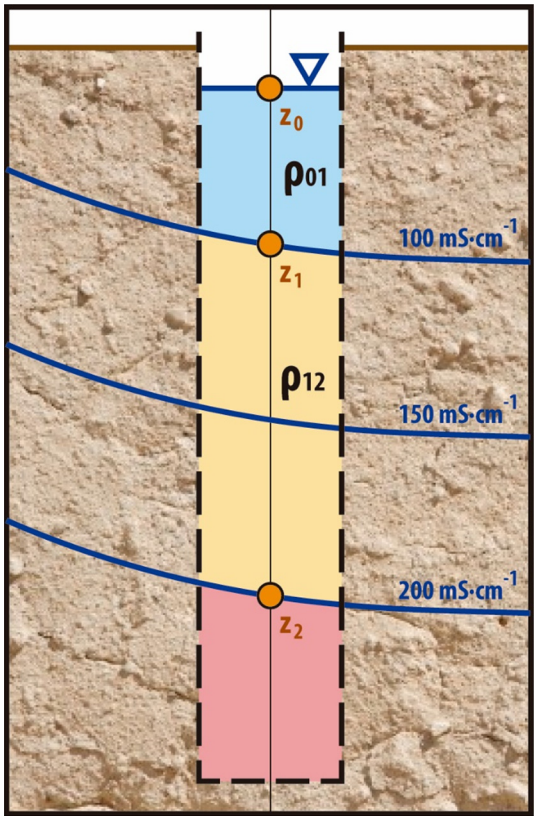

Fig. 10. Schematic of a long-screened well in which the reference surfaces utilized to carry out the correction by density contrast are shown. In the case of point wells, the situation would be similar, but the internal density surfaces would not agree with the surfaces of the mixing-zone regional mapping.

because it is considered to be practically brine. The correction of the second stretch is performed based on the thickness of the mixing zone between the surfaces of 200 mS·cm^{-1} and 100 mS·cm^{-1} and their average density. Finally, the correction in the third stretch is made by taking into account a linear gradient between the existing density in the surface of 100 mS·cm^{-1} and the density measured in the upper water of that observation point:

$$h_c = h_i + (z_1 - z_0)\frac{\rho_{01} - \rho_0}{\rho_0} + (z_2 - z_1)\frac{\rho_{12} - \rho_0}{\rho_0} \quad (3)$$

where z_1 is the depth corresponding to the 100 mS·cm^{-1} surface, ρ_{01} is the average density between z_0 and z_1, and ρ_{12} is the average density between z_1 and z_2. In the monitoring wells where the third stretch does not exist (when the internal mixing zone is close to the land surface), the correction is made by applying the density value measured at the surface to the entire freshwater column.

In this case, the corrected water head may be slightly underestimated by not correcting from 200 mS·cm^{-1} to 240 mS·cm^{-1}. However, it is very difficult to map the surface of 240 mS·cm^{-1} (with a density of 1.23 kg/L), as it is only attained in some areas of the salt flat nucleus. The mixing zone stretch in which the density/EC values change faster is between 100 and 200 mS·cm^{-1}. Farther from these surfaces, these changes are slow, diffuse and too complex to be identified.

4.2. Mixing zone hydrodynamics

In the quasi-stationary stage (Fig. 8), the effects of variable density allow us to differentiate five sectors with very different hydraulic behaviours, namely, the nucleus, internal mixing zone (IMZ), middle mixing zone (MMZ), external mixing zone (EMZ), and recharge zone. The hydrodynamics in the nucleus are controlled by convection cells that are continuously evolving. Triggered by the evaporation of brine in the surface, these convection cells become denser, collapse, and cause the upward movement of less-dense brine. The presence of low permeability layers, such as the intermediate aquitard AB, produce a vertical break in the convection cells. The lateral convection cell, which is closest to the mixing zone, is the engine of the upward flow in the IMZ, where a mixture with freshwater is produced causing the eastern part of the nucleus to have densities slightly lower than the western and middle zone (Fig. 2). In contrast, the recharge zone is primarily characterized by a downward flow of freshwater that gradually rotates and points towards the nucleus until the mixing zone is reached, where the flow ascends parallel to the principal mixing-zone surface. Finally, this groundwater ascends with a relatively high velocity to the land surface in the EMZ and especially in the MMZ. In this way, the MMZ is the zone that clearly presents the highest flow rates because the MMZ is where the flows coming from the nucleus and the recharge water merge (Fig. 2). The MMZ thus constitutes the main outflow of the domain, returning part of this water to the more surficial zone of the IMZ.

It is expected that the saline mixing zone, at least in the upper aquifer, is in equilibrium with climatic oscillations, even those of relatively short cycles (e.g., ENSO). In contrast, at depth, these zones do not show visible direct responses to short-term oscillations, as they only reflect the effects of large time-scale cycles. Additionally, stormy events may cause local to regional disturbances in the upper mixing zone, especially in the internal mixing zone.

These hydrological dynamics are consistent with the hydrogeochemical differences observed by Boutt et al. (2016) between the samples collected in the IMZ and EMZ. They are also consistent with the hydraulic response to short-term and long-term variations in precipitation and recharge regimes in both zones, as observed in the abovementioned manuscript. In the IMZ, where the flow is slow and sometimes has short path lines, precipitation events give rise to a more evident water table response than in the EMZ, where the flow is higher and a precipitation event induces a very small or inappreciable effect.

Finally, a special case of mixing zone occurs in the northeastern marginal zone, just to the North of the Soncor lagoon system, where numerous springs have been mapped (Fig. 4). The waters that come out of these springs drain to the Burro Muerto channel and finally to the Soncor lagoon system. If the mixing zone geometry of this zone (Figs. 4 and 5) is compared with those of the previously described southeastern and central-eastern areas, a large plateau can be seen, with its long axis approximately oriented in the N-S direction. Unlike the rest of the marginal zone, where the lagoons tend to be located along the central axis of the middle mixing zone (MMZ), in the Soncor system the mapped springs are not only located along this axis but also located in the internal mixing zone (IMZ). Furthermore, it should be noted that the mixing zone is always located around the salt flat nucleus, except in this area where the mixing zone moves northward and becomes much more gradual. The arrangement of these springs coincides with some of the structural planes described by Universidad de Chile (2016) or their extensions (Fig. 4B). There is a lowering of the hydraulic head along the permeable fault planes and an uprising of somewhat deeper freshwater flows that partially feed the springs. This could explain the very low water head gradients, the shallow water table and some of the hydrochemical anomalies described by other authors (Ortiz et al., 2014).

4.3. Influence of heterogeneity on mixing zone geometry

Through the 3D mapping of the mixing zone, important variations in the depth of the mixing zone have been observed along the entire eastern margin of the salt flat. Although different sensitivity analyses have been carried out, both for recharge and for hydraulic conductivity, the hydraulic conductivity of the upper aquifer is the one that shows the greatest sensitivity to the regional geometry of the saline interface. If the recharge varies within a coherent range (for example, by doubling or reducing it by half), the changes produced are very small. In this section we analyse the effects that the high-permeability layers in the top and the aquitards have on the geometry of the mixing zone.

To study the effect of a high-permeability layer on the upper part of the system, the regional 2D vertical model is used as a basis. The hydraulic conductivity values of the AB aquitard and the B aquifer were both set at 0.1 m/d to prevent further factors from coming into play. The hydraulic conductivity of the upper aquifer varied: 0.1 m/d (homogeneous case), 1 m/d, 10 m/d, and 100 m/d. These values are commonly found in the upper aquifer of the mixing zone and in the alluvial fans of the Salar de Atacama.

The results of the sensitivity analysis show that the higher the permeability of the upper aquifer is, the lower the slope is and the shallower the mixing zone becomes (Fig. 11). This occurs because the lateral-recharge freshwater flows almost entirely through this layer when there is an upper layer of very high permeability. In the lower layers, the recharge water almost does not penetrate, thus favouring the rise of the mixing zone and notably reducing its slope (Fig. 11C and D). On the other hand, when the aquifer is homogeneous, there is no preferential flow through the upper layer; thus the deep freshwater is able to maintain a higher head, thus repelling the mixing zone, reducing saltwater intrusions and moving it towards the salt flat (Fig. 11A and B). In the homogeneous case the largest slope of the interface is reached.

The hydraulic conductivity of the upper layers greatly influences the geometry of the regional saline interface. This explains the low slope and great intrusion of the mixing zone in the Salar de Atacama, unlike in previous works (Tejeda et al., 2003; Vásquez et al., 2013), where the mixing zone did not penetrate the alluvial fans and had a much higher slope. All of these studies considered a homogenous porous medium without a high-permeability top layer. Additionally, theoretical works (Fan et al., 1997; Hamann et al., 2015; Holzbecher, 2005) always addressed a homogenous case of study. Only Fan et al. (1997) made a first approximation of the effect of heterogeneity in the mixing zone by taking into account a more realistic geology, however these authors

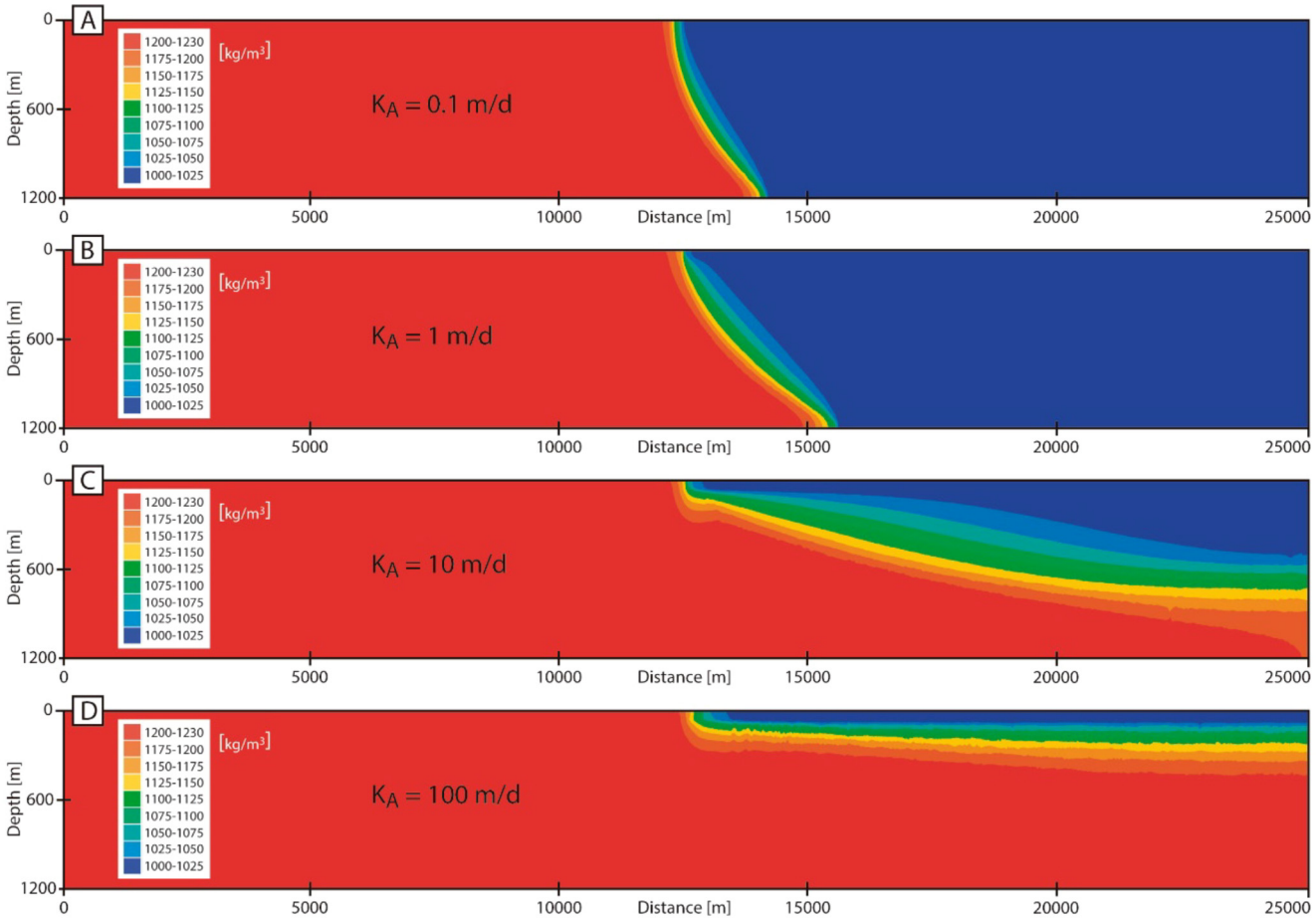

Fig. 11. Sensitivity analysis of the hydraulic conductivity of the upper aquifer. (A) 0.1 m^3/d (homogenous case). (B) 1 m^3/d. (C) 10 m^3/d. (D) 100 m^3/d. The vertical scale was exaggerated by a factor of three.

focused their efforts on explaining the free convection differences between both cases and did not focus on the geometry of the mixing zone.

The presence of aquitards can also modify the position of the mixing zone. This is because the aquitard further hinders the flow of groundwater through the deeper layers and forces the flow through the upper aquifer at up flow areas. Thus, the relative deepening and reduced thickness of the mixing zone may be observed.

The effects described above may explain the most abrupt deepening of the mixing zone observed in the central-eastern area (East of Soncor) of the Salar de Atacama (Figs. 5 and 6B). Near this zone, some studies (Cornellà et al., 2009; Ortiz et al., 2014) have described several less-permeable layers at different levels.

5. Conclusions

The two (2D) and three-dimensional (3D) geometry and hydrodynamics of the salt flat freshwater-brine mixing zone were studied, using the Salar de Atacama as case study.

The three-dimensional mapping of the actual mixing zone was carried out for the first time in a salt flat, showing the irregularities of the mixing zone in both the vertical and horizontal directions.

Using the 3D mixing zone mapping data, the application of a water head correction to the freshwater and mixed water heads in order to compensate for density variations and transform them into brine water heads was proposed to reduce the computational cost of the 3D regional models of salt flats. By applying this methodology, it was possible to reproduce the vertical fluxes in the lagoons and wetlands, which are located in the minimum regional piezometric area.

An idealized two-dimensional model of a vertical cross-section in the Salar de Atacama general structure was carried out to reproduce the mixing zone at a regional scale and to evaluate how heterogeneity affects the mixing zone geometry. The higher the permeability of the upper aquifer is, the lower the slope is and the shallower the mixing zone becomes. This occurs because the freshwater that is recharged is forced to flow through the upper aquifer and thus have a lower head at the mixing zone. Thus, hydraulic conductivity of the upper aquifer, generally constituted by karstified evaporites and alluvial deposits in the salt flats, is critical in the geometry of the resulting saline interface.

Acknowledgments

The authors acknowledge SQM for their support and for sharing data throughout the hydrogeological characterization of the SdA site. Miguel Angel Marazuela gratefully acknowledges financial support from the AGAUR (Agència de Gestió d'Ajuts Universitaris I de Recerca, Generalitat de Catalunya) and the European Union (grant number 2017FI B1 00194). The first author also gratefully acknowledges MIKE by DHI for the sponsored FEFLOW license. The authors acknowledge Juan Hidalgo for his discussion of the modelling task. Finally, we thank two anonymous reviewers for their valuable comments.

Appendix A. Supplementary data

Supplementary data associated with this article can be found, in the online version, at http://dx.doi.org/10.1016/j.jhydrol.2018.04.010.

References

Acosta, O., Custodio, E., 2008. Impactos ambientales de las extracciones de agua subterranea en el Salar del Huasco (norte de Chile). Bol. Geol. y Min. 119, 33–50.

Arriagada, C., Cobbold, P.R., Roperch, P., 2006. Salar de Atacama basin: a record of compressional tectonics in the central Andes since the mid-Cretaceous. Tectonics 25, TC1008. doi:10.1029/2004TC001770.

Bear, J., 1972. Dynamics of Fluids in Porous Media. Soil Sci. 120, 162–163. http://dx.doi.org/10.1097/00010694-197508000-00022.

Bookhagen, B., Strecker, M.R., 2008. Orographic barriers, high-resolution TRMM rainfall, and relief variations along the eastern Andes. Geophys. Res. Lett. 35, L06403. http://dx.doi.org/10.1029/2007GL032011.

Boutt, D.F., Hynek, S.A., Munk, L.A., Corenthal, L.G., 2016. Rapid recharge of fresh water to the halite-hosted brine aquifer of Salar de Atacama, Chile. Hydrol. Process. 30, 4720–4740. http://dx.doi.org/10.1002/hyp.10994.

Corenthal, L.G., Boutt, D.F., Hynek, S.A., Munk, L.A., 2016. Regional groundwater flow and accumulation of a massive evaporite deposit at the margin of the Chilean Altiplano. Geophys. Res. Lett. 43, 8017–8025. http://dx.doi.org/10.1002/2016GL070076.

Cornellà, O., Salas, J., Aravena, R., Guzmán, E., Guimerà, J., Tore, C., Von Igel, W., Henríquez, A., Fock, A., 2009. Hidrogeologia de los sistemas lagunares del margen E del Salar de Atacama. In: XII Congreso Geológico Chileno. Santiago de Chile, pp. 1–4.

Custodio, E., Bruggeman, G.A., 1987. Groundwater problems in coastal areas. Studies and reports in hydrology. UNESCO.

Custodio, E., Llamas, M.R., 1976. Hidrología Subterránea (T.2), ed. Omega, p. 1224.

Dentz, M., Tartakovsky, D.M., Abarca, E., Guadagnini, A., Sanchez-Vila, X., Carrera, J., 2006. Variable-density flow in porous media. J. Fluid Mech. 561, 209–235. http://dx.doi.org/10.1017/S0022112006000668.

Diersch, H.-J.G., 2014. FEFLOW: Finite Element Modeling of Flow, Mass and Heat Transport in Porous and Fractured Media, FEFLOW: Finite Element Modeling of Flow, Mass and Heat Transport in Porous and Fractured Media. doi:10.1007/978-3-642-38739-5.

Duffy, C.J., Al-Hassan, S., 1988. Groundwater circulation in a closed desert basin: Topographic scaling and climatic forcing. Water Resour. Res. 24, 1675–1688. http://dx.doi.org/10.1029/WR024i010p01675.

Fan, Y., Duffy, C.J., Oliver, D.S., 1997. Density-driven groundwater flow in closed desert basins: Field investigations and numerical experiments. J. Hydrol. 196, 139–184. http://dx.doi.org/10.1016/S0022-1694(96)03292-1.

Gajardo, G.M., Beardmore, J.A., 2012. The brine shrimp Artemia: Adapted to critical life conditions. Front. Physiol. 3, article 185. doi:10.3389/fphys.2012.00185.

Garreaud, R.D., Molina, A., Farias, M., 2010. Andean uplift, ocean cooling and Atacama hyperaridity: a climate modeling perspective. Earth Planet. Sci. Lett. 292, 39–50. http://dx.doi.org/10.1016/j.epsl.2010.01.017.

Glover, R.E., 1959. The pattern of fresh-water flow in a coastal aquifer. J. Geophys. Res. 64 (4), 457–459. http://dx.doi.org/10.1029/JZ064i004p00457.

Hamann, E., Post, V., Kohfahl, C., Prommer, H., Simmons, C.T., 2015. Numerical investigation of coupled density-driven flow and hydrogeochemical processes below playas. Water Resour. Res. 51, 9338–9352. http://dx.doi.org/10.1002/2015WR017833.

Hardie, L.A., 1991. On the significance of evaporites. Annu. Rev. Earth Planet. Sci. 19, 131–168.

Hartley, A.J., Chong, G., 2002. Late Pliocene age for the Atacama Desert: Implications for the desertification of western South America. Geology 30, 43–46. http://dx.doi.org/10.1130/0091-7613(2002) 030<0043:LPAFTA>2.0.CO;2.

Hayashi, M., 2004. Temperature-electrical conductivity relation of water for environmental monitoring and geophysical data inversion. Environ. Monit. Assess. 96, 119–128. http://dx.doi.org/10.1023/B:EMAS.0000031719.83065.68.

Holzbecher, E., 2005. Groundwater flow pattern in the vicinity of a salt lake. Hydrobiologia 532, 233–242.

Hubbert, M.K., 1940. The theory of groundwater motion. Eos. Trans. Am. Geophys. Union 21, 648. http://dx.doi.org/10.1029/TR021i002p00648-1.

IDAEA-CSIC, 2017. Cuarta actualización del modelo hidrogeológico del Salar de Atacama. Accessed by permision.

Iribar, V., Carrera, J., Custodio, E., Medina, A., 1997. Inverse modelling of seawater intrusion in the Llobregat delta deep aquifer. J. Hydrol. 198, 226–244. http://dx.doi.org/10.1016/S0022-1694(96)03290-8.

Jellison, R., Macintyre, S., Millero, F.J., 1999. Density and conductivity properties of Na-CO3-Cl-SO4 brine from Mono Lake, California. USA. Int. J. Salt Lake Res. 8, 41–53.

Jordan, T.E., Mpodozis, C., Muñoz, N., Blanco, N., Pananont, P., Gardeweg, M., 2007. Cenozoic subsurface stratigraphy and structure of the Salar de Atacama Basin, northern Chile. J. South Am. Earth Sci. 23, 122–146. http://dx.doi.org/10.1016/j.jsames.2006.09.024.

Kampf, S.K., Tyler, S.W., 2006. Spatial characterization of land surface energy fluxes and uncertainty estimation at the Salar de Atacama, Northern Chile. Adv. Water Resour. 29, 336–354. http://dx.doi.org/10.1016/j.advwatres.2005.02.017.

Kampf, S.K., Tyler, S.W., Ortiz, C.A., Muñoz, J.F., Adkins, P.L., 2005. Evaporation and land surface energy budget at the Salar de Atacama, Northern Chile. J. Hydrol. 310, 236–252. http://dx.doi.org/10.1016/j.jhydrol.2005.01.005.

Kesler, S.E., Gruber, P.W., Medina, P.A., Keoleian, G.A., Everson, M.P., Wallington, T.J., 2012. Global lithium resources: Relative importance of pegmatite, brine and other deposits. Ore Geol. Rev. 48, 55–69. http://dx.doi.org/10.1016/j.oregeorev.2012.05.006.

Kohfahl, C., Post, V.E.A., Hamann, E., Prommer, H., Simmons, C.T., 2015. Validity and slopes of the linear equation of state for natural brines in salt lake systems. J. Hydrol. 523, 190–195. http://dx.doi.org/10.1016/j.jhydrol.2015.01.054.

Lu, C., Werner, A.D., Simmons, C.T., Luo, J., 2015. A Correction on Coastal Heads for Groundwater Flow Models. Groundwater 53, 164–170. http://dx.doi.org/10.1111/gwat.12172.

Lusczynski, N.J., 1961. Head and Flow of Ground Water of Variable Density. J. Geophys. Res. 66, 4247–4256. http://dx.doi.org/10.1029/JZ066i012p04247.

Maas, C., Emke, M.J., 1989. Solving varying density groundwater problems with a single density computer program. In: 10th SWIM, Ghent.

Mpodozis, C., Arriagada, C., Basso, M., Roperch, P., Cobbold, P., Reich, M., 2005. Late Mesozoic to Paleogene stratigraphy of the Salar de Atacama Basin, Antofagasta, Northern Chile: Implications for the tectonic evolution of the Central Andes. Tectonophysics 399, 125–154. http://dx.doi.org/10.1016/j.tecto.2004.12.019.

Munk, L.A., Hynek, S.A., Bradley, D., Boutt, D.F., Labay, K., Jochens, H., 2016. Lithium brines: a global perspective. Rev. Econ. Geol. 18, 339–365.

Muñoz-Pardo, J.F., Ortiz-Astete, C.A., 2004. Funcionamiento hidrogeológico del acuífero del núcleo del salar de Atacama, Chile. Ing. Hidráulica en Mex. XIX 69–81.

Nield, D.A., Simmons, C.T., Kuznetsov, A.V., Ward, J.D., 2008. On the evolution of salt lakes: episodic convection beneath an evaporating salt lake. Water Resour. Res. 44, W02439. http://dx.doi.org/10.1029/2007WR006161.

Ortiz, C., Aravena, R., Briones, E., Suárez, F., Tore, C., Muñoz, J.F., 2014. Sources of surface water for the Soncor ecosystem, Salar de Atacama basin, northern Chile. Hydrol. Sci. J. 59, 336–350. http://dx.doi.org/10.1080/02626667.2013.829231.

Oude-Essink, G.H.P., 2001. Improving fresh groundwater supply—problems and solutions. Ocean Coast. Manag. 44, 429–449. http://dx.doi.org/10.1016/S0964-5691(01)00057-6.

Oude-Essink, G.H.P., Boekelman, R.H., 1996. Problems with large-scale modelling of salt water intrusion in 3D. In: 14th SWIM, Malmö.

Pananont, P., Mpodozis, C., Blanco, N., Jordan, T.E., Brown, L.D., 2004. Cenozoic evolution of the northwestern Salar de Atacama Basin, northern Chile. Tectonics 23, 1–19. http://dx.doi.org/10.1029/2003TC001595.

Pool, M., Carrera, J., 2011. A correction factor to account for mixing in Ghyben-Herzberg and critical pumping rate approximations of seawater intrusion in coastal aquifers. Water Resour. Res. 47, W05506. http://dx.doi.org/10.1029/2010WR010256.

Post, V., Kooi, H., Simmons, C., 2007. Using hydraulic head measurements in variable-density ground water flow analyses. Ground Water 45, 664–671. http://dx.doi.org/10.1111/j.1745-6584.2007.00339.x.

Rio Chilex S.A, 1997. Evaluación hidrogeológica acuífero sector norte Salar de Atacama. URL http://sad.dga.cl/ipac20/ipac.jsp?session=15Y54918K1790.3317420&menu=search&aspect=subtab39&npp=10&ipp=20&spp=20&profile=cirh&ri=&term=Evaluación+hidrogeológica+acuífero+sector+norte&index=.GW&x=0&y=0&aspect=subtab39. Last Access: 01-09-2017.

Risacher, F., Alonso, H., Salazar, C., 2003. The origin of brines and salts in Chilean salars: a hydrochemical review. Earth-Sci. Rev. 63, 249–293. http://dx.doi.org/10.1016/S0012-8252(03)00037-0.

Rockwood Lithium, 2015. Estudio de Impacto ambiental Proyecto modificaciones y mejoramiento del sistema de pozas de evaporación solar en el Salar de Atacama. http://seia.sea.gob.cl/expediente/ficha/fichaPrincipal.php?modo=ficha&id_expediente=3788682. Last Access: 01-09-2017.

Rosen, M.R., 1994. The importance of groundwater in playas: A review of playa classifications and the sedimentology and hydrology of playas. Geol. Soc. Am. Spec. Pap. 289, 1–18. http://dx.doi.org/10.1130/SPE289-p1.

Rushton, K.R., 1980. Differing positions of saline interfaces in aquifers and observation boreholes. J. Hydrol. 48, 185–189.

Salas, J., Guimerà, J., Cornellà, O., Aravena, R., Guzmán, E., Tore, C., Von Igel, W., Moreno, R., 2010. Hidrogeologia del sistema lagunar del margen este del Salar de Atacama (Chile). Bol. Geol. y Min. 121, 357–372.

Tejeda, I., Cienfuegos, R., Muñoz, J.F., Durán, M., 2003. Numerical Modeling of Saline Intrusion in Salar de Atacama. J. Hydrol. Eng. 8, 25–34. http://dx.doi.org/10.1061/(ASCE)1084-0699(2003) 8:1(25).

Tyler, S.W., Muñoz, J.F., Wood, W.W., 2006. The response of playa and sabkha hydraulics and mineralogy to climate forcing. Ground Water 44 (3), 329–338. http://dx.doi.org/10.1111/j.1745-6584.2005.00096.x.

Universidad de Chile, 2016. Estudio estructural Zona Marginal, sector oriente del Salar de Atacama. Internal report of Sociedad Química y Minera de Chile S.A. (SQM).

USGS, 2017. Minneral commodities summary [WWW Document]. URL https://minerals.usgs.gov/minerals/pubs/mcs/.

Vásquez, C., Ortiz, C., Suárez, F., Muñoz, J.F., 2013. Modeling flow and reactive transport to explain mineral zoning in the Atacama salt flat aquifer. Chile. J. Hydrol. 490, 114–125. http://dx.doi.org/10.1016/j.jhydrol.2013.03.028.

Vázquez-Suñé, E., Abarca, E., Carrera, J., Capino, B., Gámez, D., Pool, M., Simó, T., Batlle, F., Niñerola, J.M., Ibañez, X., 2006. Groundwater modelling as a tool for the European Water Framework Directive (WFD) application: the Llobregat case. Phys. Chem. Earth 31, 1015–1029. http://dx.doi.org/10.1016/j.pce.2006.07.008.

Vikström, H., Davidsson, S., Höök, M., 2013. Lithium availability and future production outlooks. Appl. Energy 110, 252–266. http://dx.doi.org/10.1016/j.apenergy.2013.04.005.

Werner, A.D., Bakker, M., Post, V.E.A., Vandenbohede, A., Lu, C., Ataie-Ashtiani, B., Simmons, C.T., Barry, D.A., 2013. Seawater intrusion processes, investigation and management: Recent advances and future challenges. Adv. Water Resour. 51, 3–26. http://dx.doi.org/10.1016/j.advwatres.2012.03.004.

Wood, W.W., Sanford, W.E., 1990. Ground-water control of evaporite deposition. Econ. Geol. 85, 1226–1235. http://dx.doi.org/10.2113/gsecongeo.85.6.1226.

Wooding, R.A., Tyler, S.W., White, I., 1997. Convection in groundwater below an evaporating Salt Lake: 1. Onset of instability. Water Resour. Res. 33, 1199–1217. http://dx.doi.org/10.1029/96WR03533.

Yechieli, Y., Wood, W.W., 2002. Hydrogeologic processes in saline systems: Playas, sabkhas, and saline lakes. Earth-Sci. Rev. 58, 343–365. http://dx.doi.org/10.1016/S0012-8252(02)00067-3.